





Article

Formation of Vibration Fields for a Mechatronic Platform Driven by Dual Asynchronous Motors

Alexander L. Fradkov ^{1,2}, Boris Andrievsky ^{1,2,*}, Olga P. Tomchina ³ and Iuliia Zaitceva ^{1,2}

- ¹ Control of Complex Systems Laboratory, Institute for Problems in Mechanical Engineering of the Russian Academy of Sciences (IPME RAS), 61 Bol'shoy Pr. V.O., 199178 Saint Petersburg, Russia; fradkov@mail.ru or alf@ipme.ru (A.L.F.); y.zaitseva@spbu.ru (I.Z.)
- ² Faculty of Mathematics and Mechanics, Saint Petersburg University, Stary Peterhof, Universitetsky Prospekt, 198504 Saint Petersburg, Russia
- ³ Saint Petersburg State University of Architecture and Civil Engineering, 4, 2nd Krasnoarmeiskaya Str., 190005 Saint Petersburg, Russia; otomchina@mail.ru
- * Correspondence: b.andrievsky@spbu.ru, boris.andrievsky@gmail.com or abr@ipme.ru; Tel.: +7-(812)-321-4776

Abstract: This paper investigates the formation of vibration fields in a mechatronic setup driven by dual induction motors, relying on the controlled synchronization of unbalanced rotors. The proposed algorithm enables precise control over rotor speeds and phase shifts. Experimental results from a multi-resonance vibration laboratory setup demonstrate this approach's ability to form the vibration fields. The ability to control these fields is crucial for applications such as vibratory transportation and the mixing of bulk materials. The results obtained can ensure a diverse picture of the complex trajectories of motion for various points of the platform, primarily in the screens, making various useful effects for vibration technologies. Additionally, the practical value of this research is that in the case of double synchronous mode the ordinate of the lower point of the trajectory is lower than in the case of single synchronous mode, which improves the efficiency of unloading and prevents congestion formation. The experimental data highlight the practical advantages and potential improvements in efficiency and reliability offered by this method.

Keywords: vibration machines; phase shift; vibration field; synchronization



Citation: Fradkov, A.L.; Andrievsky, B.; Tomchina, O.P.; Zaitceva, I. Formation of Vibration Fields for a Mechatronic Platform Driven by Dual Asynchronous Motors. *Electronics* **2024**, *13*, 3165. <https://doi.org/10.3390/electronics13163165>

Academic Editor: Jianguo Zhu

Received: 11 July 2024

Revised: 8 August 2024

Accepted: 9 August 2024

Published: 10 August 2024



Copyright: © 2024 by the authors. Licensee MDPI, Basel, Switzerland. This article is an open access article distributed under the terms and conditions of the Creative Commons Attribution (CC BY) license (<https://creativecommons.org/licenses/by/4.0/>).

1. Introduction

Vibration machines (VMs) and technologies play a crucial role across various industries, including manufacturing and agriculture. It is challenging to envision conducting tasks such as material separation, vibratory transportation, grinding, rolling, mixing, compaction, pile driving, and more without the aid of VMs and associated devices [1]. Their utilization not only yields significant technical and economic benefits but also contributes to enhancing working conditions.

Among the primary sources for inducing oscillations in vibration machines, unbalanced actuators stand out as the most commonly employed [2–4]. These actuators find application in various technologies such as vibratory conveyors, lifters, screens, and rammers, where circular, elliptical, or directional vibrations are necessary. Circular vibrations are typically produced by an unbalanced rotor, or two unbalanced rotors, revolving in phase in the same direction, or anti-phase—in the opposite directions. When there exists a phase discrepancy between the driving forces of two-shaft vibration actuators, elliptical oscillations manifest themselves.

In the VM applications for tasks like screening, crushing, and bulk material transportation, enhancing productivity often hinges on maintaining a stable synchronous rotation mode of unbalanced rotors (vibration actuators). The foundations of VM synchronization theory were established in the 1960s by I.I. Blekhman [3,5,6]. This theory laid the groundwork for synchronization mechanisms in traditional rigid or flexible transmissions,

gradually showing the advantages of vibration equipment powered by two or more actuators. Such systems enable the vibration machine to produce various trajectories through a synchronization phenomenon, see [4]. The multiple synchronization modes are based on the self-synchronization phenomenon, wherein vibration actuators rotate at average angular velocities that are multiples of each other. This mode leads to more efficient vibrating behavior, especially in challenging tasks such as transporting dusty, sticky, or wet granular media.

Studying the flow field variation in twin-roll strip casting processes induced by oscillating rollers was carried out in [7]. This research is focused on achieving a homogeneous distribution of strip impurities, reducing grain size, and thereby enhancing strip quality through the adoption of the proposed vibrating casting.

Electro-hydraulic vibration equipment finds extensive application in various vibration environment simulation tests. Liu et al. [8] addressed the problems related to bandwidth, waveform distortion control, stability, offset control, and complex waveform generation in high-frequency vibration conditions.

Shi et al. [9] concentrated on the vibration synchronization of mechanical structures propelled by two vibroactuators. They introduced a synchronization mechanism combining space and plane patterns through the extension of vibrator installation to arbitrary directions in spatial axes. Altshul et al. [10] and Panovko et al. [11] examined variations in the arrangement of technological loads on the machine's working body. It was demonstrated how shifts in the load center from the machine's constructive axis of symmetry lead to changes in resonant frequencies and mutual phasing of unbalances, and the feasibility of controlling resonant VMs by adjusting vibro-actuator power frequencies to compensate for uncontrolled load shifts was discussed.

In the domain of dual-mass vibration systems, Liu et al. [12] investigated vibratory synchronization phenomena driven by two actuators. They employed averaging methods to deduce synchronization and stability criteria in synchronous states, quantitatively analyzing parameters such as actuator rotational speeds, phase differences, and responses in sub-resonant and super-resonant states, accompanied by an engineering example. Using asymptotic and average methods, Zhang et al. [13] derived theoretical conditions for implementing multiple synchronization and stability, with a particular focus on analyzing synchronization for four actuators. Leniowska and Sierze [14] studied the controlled vibration damping of a round plate utilizing a controller with phase shift adjustment in the feedback loop. A novel controller was proposed, combining regulator structures with positive position feedback and strain rate feedback. Experimental studies involve measuring plate vibrations using a laser vibrometer, with a control signal applied to the plate via a Macro Fiber Composite (MFC) disk affixed to its center. Their findings demonstrate the feasibility of employing this solution to mitigate plate vibration effectively.

The phenomenon of transporting solid and granular bodies over oscillating rough surfaces has found numerous technical applications. Vibrational movement arises from an average directed motion of material particles relative to horizontally oscillating uniformly rough surfaces, stemming from the asymmetry of surface oscillation shapes, as expressed in the inequality of time intervals between consecutive extrema of surface acceleration oscillations, see [15–17]. Theoretical investigations by Blekhman et al. [17] focused on the oscillatory transportation of solid particles over flat surfaces under non-translational vibrations. This work, with experimental validation conducted on a vibration platform, revealed that the existing theory, with additional parameters introduced, can effectively set up the speed of vibrational transportation. Advancements towards intelligent technological systems involve employing mechatronics principles, particularly computer-controlled vibration setups with feedback mechanisms [17].

The introduction of feedback control in manipulating the vibration field has been addressed by Fradkov et al. [18], who were initially focused on simple synchronization cases. However, it became clear that the appearance of multiple synchronous modes introduces asymmetry, enhancing vibration movement efficacy by creating complex trajectories for

rotors and carrier bodies. Nevertheless, the stability of multiple-synchronous movements remains a challenge, necessitating further exploration into controlling vibration using feedback control for vibroactuators.

This paper studies the vibrational system controlled by the method proposed by Fradkov et al. [18] from the perspective of creating the various vibration fields for the operational platform, driven by the actuators with unbalanced rotors. Experimental validation conducted at the Multi-resonance Mechatronic Laboratory Setup confirms the approach's efficacy, demonstrating its practical applicability in controlling the type of vibration fields of the working platform, crucial for bulk material transportation processes.

The subsequent sections are structured as follows: Section 2 briefly outlines the Mechatronic Setup SV-2M utilized for experiments. Section 3 presents the bidirectional control law for multiple synchronization of the unbalanced rotors. The experimental results along with the data processing algorithm are presented in Section 4. Concluding remarks and future work intentions are outlined in Section 5.

2. Experimental Mechatronic Setup SV-2M

2.1. General Description

The Multiresonance Mechatronic Laboratory Setup (MMLS) SV-2M of the IPME RAS, used in this work for experimental investigations, provides broad research capabilities; see [18] for details.

A vibration complex SV-2M is a nonlinear electromechanical system equipped with two induction motors (IMs) with unbalanced rotors [18]. The photography of the set-up SV-2M is depicted in Figure 1. The photo on the left gives a general view of the complex, which includes a control computer with a monitor, a power supply unit for the stand with electronic components, and the mechanical part of the setup, bounded by a fence. This unit is shown in more detail in the photo on the right, which shows two induction motors with unbalanced rotors mounted on a massive base and a spring-loaded working platform.

To control oscillations, including their frequencies and phasing (specifically, for ensuring multiple synchronization), and to collect data, the setup is designed as a mechatronic system, which includes sensors for measurement the angles and positions of various elements, and the sensors' readings are transmitted to a control computer. In feedback mode, the computer generates control signals, which are sent through frequency converters to the induction motors driving the unbalanced rotors.

The sensors' nomenclature is as follows. Optical motion sensors *DFRobot Smart Grayscale Sensors* are installed for obtaining information about the linear and angular coordinates of the 6-degrees-of-freedom platform. In the SV-2M, the analog sensor outputs are used, which are fed to the analog I/O board *PCI826* for transferring measured data to the PC. Measuring characteristics of sensors are demonstrated in Figure 2 as mappings of distances between the basement and the corresponding points of the platform l_i , $i = 1, 2, \dots, 6$ to the digital numbers at the outputs L_i of the corresponding channels of the *PCI826* driver, which transferred to the computer. The location of linear displacement sensors on the main platform is shown schematically in Figure 3. Sensors s_1 – s_3 measure the position of the main platform in the vertical plane, and sensors s_4 – s_6 measure its position in the horizontal plane; sensors s_4 and s_5 measure displacement along the X axis, sensor s_6 measures displacement along the Y axis. In Figure 3, the numbers #1 ... #4 indicate the points of interest for the following study of the platform vibrations. In Figure 3, numbers #1 ... #4 indicate the points of interest of the platform for the succeeding study of its vibrations. Two velocity sensors with *Autonics E30S4-1000-6L* encoders, having a resolution of 4000 pulses/revolution, are mounted for measuring rotation angles φ_l , φ_r of unbalanced *left* and *right* (conventionally) rotors.

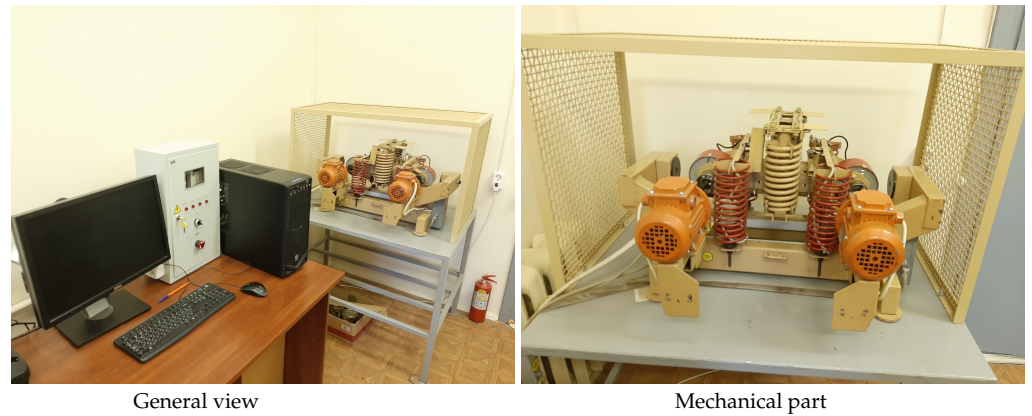


Figure 1. Photography of the set-up SV-2M.

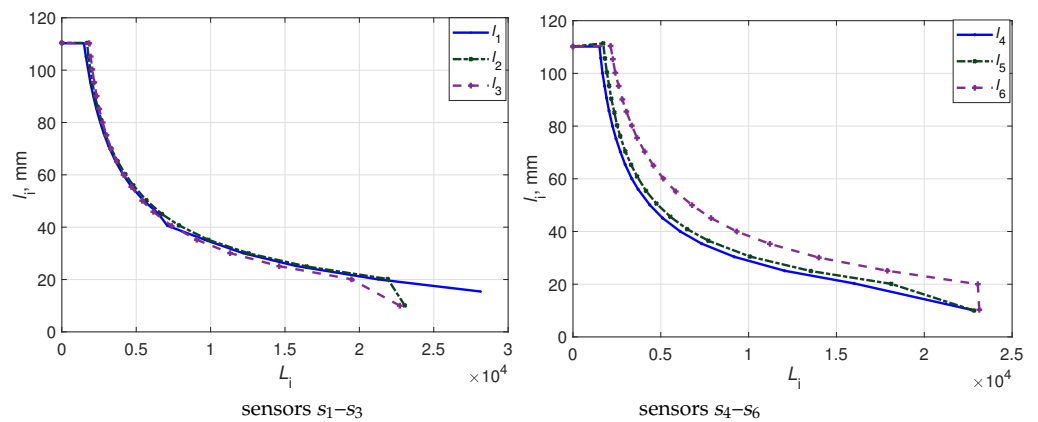


Figure 2. Measuring characteristics of sensors s_1-s_6 .

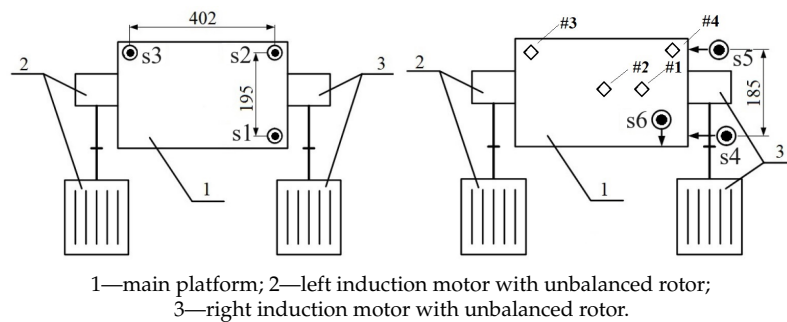


Figure 3. Schematic diagram of the setup (top view) and location of sensors s_1-s_6 on the main platform.

2.2. Modeling the SV-2M Mechanical Part

To give a clearer impression of the stand mechanics, following [18,19], we briefly present its description. The kinematic scheme of the two-rotor vibration unit with an attached load is given in (Figure 2 in [18]). Employing the standard Lagrangian formalism, in [18,19] the dynamical model of the setup mechanical part was developed. It is a substantially nonlinear system of sixth-order differential equations in which the input quantities are two torques applied to the rotors by induction motors. Based on this model, the following relations for the setup resonant frequencies $\omega_{res,1}$, $\omega_{res,2}$ can be approximately found as follows [18–20]:

$$\omega_{res,1} = \sqrt{c_{02}/(m_0 + m_p)}, \quad \omega_{res,2} = \sqrt{c_{05}/m_p}, \quad (1)$$

where c_{02} , c_{05} denote stiffness coefficients of the elastic support elements along the vertical and horizontal axes (respectively), m stands for the rotor mass, m_p is the mass of the platform, see [18,19] for details.

Although the system dynamics are very complex, the equations contain a large number of difficult-to-determine parameters, and also that this model does not describe the drive dynamics, in [18] it is shown that at the stage of a rotor control system design, it is advisable to use a simplified model based on the so-called “averaging property”, see [1], which manifests itself for frequencies above 30 rad/s. As follows from this property, fast oscillatory components are averaged, and only “slow” movements can be taken into account for revolving rotors. Based on this approach, the following simplified model of the setup was adopted in [18] at the controller design stage

$$W_d(s) = \left\{ \frac{\omega}{u} \right\} = \frac{b_0}{a_0s^2 + a_1s + 1}, \quad (2)$$

where b_0 , a_0 , a_1 denote the parameters of the drive model. These parameters were estimated in [18] based on the standard non-recursive least-square identification procedure. Model (2) was used in [18] for the control law synthesizing and the linearized system stability analysis.

3. Bidirectional Control Law for Multiple Synchronization of Unbalanced Rotors

In [18], the problem of controlled synchronization for unbalanced rotors’ phase shift was considered. The control law presented in [18] for the multiple synchronization of unbalanced rotors has the following form:

$$\omega_r^*(t) = \kappa^{-1}\omega_l^*(t), \quad (3)$$

$$e_{\omega_l}(t) = \omega_l^*(t) - \omega_l(t), \quad e_{\omega_r}(t) = \omega_r^*(t) - \omega_r(t), \quad (4)$$

$$\dot{\sigma}_{\omega_l} = e_{\omega_l}, \quad u_{\omega_l} = K_{i\omega_l}\sigma_{\omega_l} + K_{p\omega_l}e_{\omega_l}, \quad (5)$$

$$\dot{\sigma}_{\omega_r} = e_{\omega_r}, \quad u_{\omega_r} = K_{i\omega_r}\sigma_{\omega_r} + K_{p\omega_r}e_{\omega_r}, \quad (6)$$

$$\psi = \kappa\varphi_r - \varphi_l, \quad (7)$$

$$e_\psi(t) = \psi^*(t) - \psi(t), \quad (8)$$

$$\dot{\sigma}_\psi = e_\psi, \quad u_\psi = -K_{i,\psi}\sigma_\psi + K_{p,\psi}e_\psi, \quad (9)$$

$$u_l = u_{\omega_l} + u_\psi, \quad u_r = u_{\omega_r} - u_\psi, \quad (10)$$

where $\omega_r^*(t)$, $\omega_l^*(t)$ are the motors’ reference velocities; κ is the normalization coefficient; $e_{\omega_l}(t)$, $e_{\omega_r}(t)$ are the errors of motor velocities; σ_{ω_l} , σ_{ω_r} , σ_ψ are the integrals or tracking errors e_{ω_l} , e_{ω_r} , e_ψ (respectively), which are used in the PI-controllers; PI-controllers for the velocities of the left and right motors are described by (5), (6), respectively, where $K_{i\omega_l}$, $K_{i\omega_r}$ are for the integral, and $K_{p\omega_l}$, $K_{p\omega_r}$ are for the proportional controller gains; in (7), $\varphi_r(t)$ and $\varphi_l(t)$ are the phase angles of the rotors, and $\psi(t)$ denotes the normalized phase shift between the rotors; the phase shift error is denoted by e_ψ , where $\psi^*(t)$ is the reference phase shift angle between the rotors; $u_l(t)$ and $u_r(t)$ in (10) denote the control signals applied to the left and right drive systems produced by the corresponding PI-controllers.

In [18], the linearized system stability analysis for model (2) and control law (3)–(10) was performed. The results were confirmed by the computer simulations and the numerous real-world experiments on the setup SV-2M.

4. Experimental Results

In the present paper, the experimental study results of [18] are extended to studying the corresponding vibration platform deflections and summarized in the form of the spectral densities of selected points of platform movements and the “vibration fields” of the platform.

The main aim of this study is to demonstrate the vibration fields by the example of moving the platform points #1–#4 (see Figure 3).

4.1. Data Processing Algorithm

The following processing algorithm is implemented to obtain the type of vibration fields based on experimental data.

Platform position sensors data are acquired with a sampling interval T_s and saved to a file for further offline post-processing. Given the range of platform oscillation frequencies, an interval of $T_s = 0.002$ s was chosen, corresponding to a Nyquist frequency $\omega_N \approx 3100$ rad/s. At the end of the experiment, the data array was saved to the hard disk drive (HDD) for subsequent processing.

Data acquisition from the sensors is performed using Simulink Desktop Real-Time toolbox, which includes Simulink I/O driver blocks enabling closed-loop control of physical systems from a desktop computer, allowing connections to sensors, actuators, and other devices. Data Type Conversion blocks are used to convert the measurements to MATLAB *double* type data for further processing. Simulink blocks “To Workspace” are used to save the data to the workspace. After the experiment, using the MATLAB save routine, the data obtained are saved on the HDD in the form of a MATLAB mat-file.

Since the measurement characteristics of optical sensors s_1, \dots, s_6 , given by $l_i = f_i(L_i)$, $i = 1, \dots, 6$, are close to the inversely proportional mappings presented in Figure 2, the displacements $l_i(t_k)$, at times $t_k = kT_s$, $k = 1, 2, \dots$ of the corresponding platform points s_1, \dots, s_6 are restored based on the sensor readings. Before the experiments, optical sensors position had been calibrated to obtain their real measurement characteristics and the results were tabulated in 20 points inside the working range (see Figure 2). Sensor measurements sometimes include random spikes, which are erroneous readings outside the normal range. Therefore, these anomalies were removed before further processing. For this purpose, each sensor’s entire array of measurements was subjected to statistical analysis using partitions the values of $l_i(t_k)$ into M bins, and returning the count in each bin. $M = 1000$ bins was set for data processing. Next, values that occur in the measurement array less than the specified threshold value n_{\min} are selected ($n_{\min} = 10$ was set) and are replaced by the arithmetic mean of the measurement array. To recover displacement values $l_i(t_k)$ from sensor signals $L_i(t_k)$, an spline-interpolation procedure was used on the every data processing step $k = 0, 1, \dots$.

For the obtained data arrays, spectrograms and the filtered centered platform displacements are calculated and displayed to the user by the following sequence of operations.

1. Find time-average values of the displacement processes of the sensor positions.
2. Apply Discrete Fourier Transform (DFT) to the resulting centered processes $\bar{l}_i(k)$.
3. Calculate the squared \mathcal{Y} modulus, normalized by the number of points.
4. Convert the resulting complex-valued array of images \mathcal{Y} into the array of spectral densities $S_i(\omega)$.
5. Select frequencies ω_j , $j = 1, 2, 3$, where $S_i(\omega)$ bursts were observed.
6. Clear sensor measurements using the DFT concerning $\bar{l}_i(k)$.
7. Find the set of frequencies Ω in the vicinities of ω_j such as: $\Omega = \bigcup_{j=1}^3 (|\omega - \omega_j| \leq \Delta\omega)$, where $\Delta\omega > 0$ is a chosen bandwidth relative to the peak frequencies ω_j .
8. Form new complex-valued arrays $\tilde{\mathcal{Y}}_i(\omega)$ by zeroing the values of $\mathcal{Y}_i(\omega)$ except those that correspond to the frequencies from Ω , which values are copied from $\mathcal{Y}_i(\omega)$, and their spectral densities $\tilde{S}_i(\omega)$ were found.
9. Find $l_i(k)$ as the complex-valued inverse Fourier transforms to $\tilde{\mathcal{Y}}_i(\omega)$.
10. Find the real part of $l_i(k)$.
11. Apply the Inverse Discrete Fourier Transform (IDFT) to $\tilde{\mathcal{Y}}_i(\omega)$.
12. Calculate the filtered centered platform displacements $\tilde{l}_i(k)$ as $\tilde{l}_i(k) = \text{real}(l_i(k)) \|\mathcal{S}_i(\omega)\| / \|\tilde{\mathcal{S}}_i(\omega)\|$, where $\|\cdot\|$ stands for the Euclidean norm of the complex-valued vector argument.

As an example of the described procedure application, consider the case of filtering data of $l_2(t)$, $l_5(t)$, obtained for $\omega_l = 80$ rad/s, $\omega_r = 40$ rad/s, $\psi = \pi/2$, taking $\omega_j \in \{20.5, 40, 80\}$ rad/s, $\Delta\omega = 5$ rad/s, and $\Delta\omega = 25$ rad/s. The resulting time histories for $l_i(t_k)$, $i \in \{2, 5\}$ along with $\tilde{l}_i(t_k)$ are depicted in Figure 4. The graphs obtained for different values of $\Delta\omega$ show the influence of this parameter on the result of measurement filtering. The choice of frequency filter parameters is always a compromise between noise alleviation and possible signal distortion in the area of essential frequencies. The decision is assigned to the researcher, making it based on the study of processes for specific conditions.

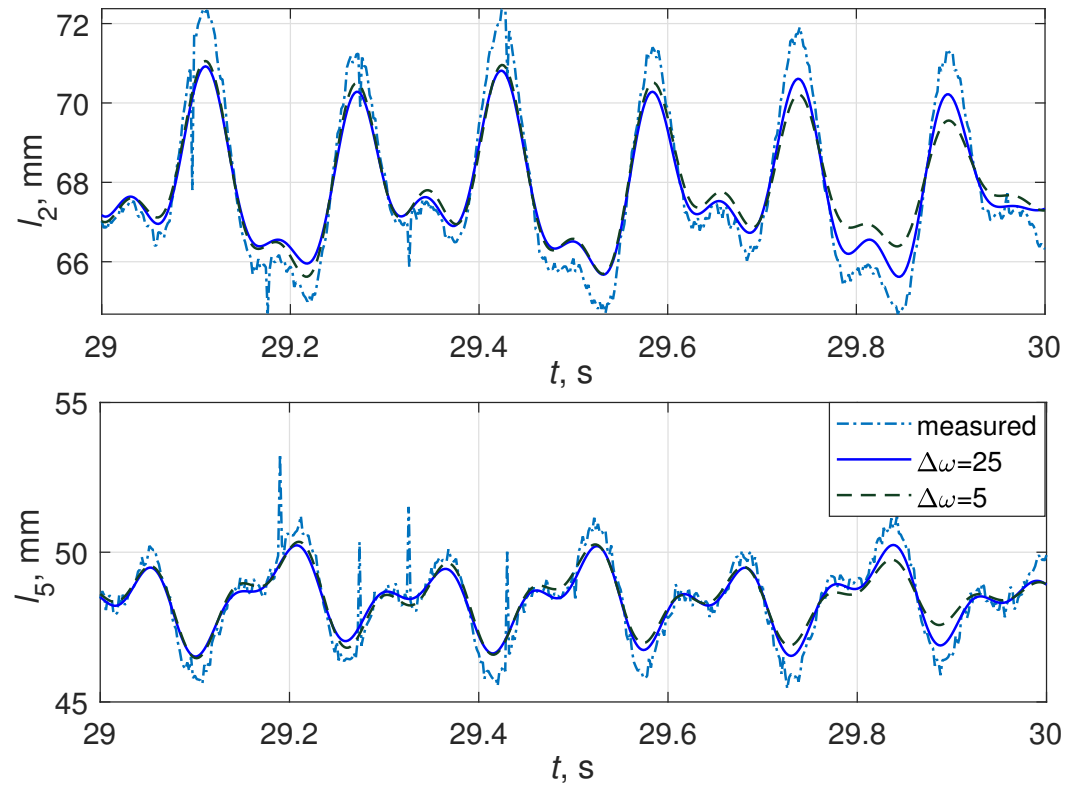


Figure 4. Time histories of measured (dash-dot line) and filtered $l_2(t)$, $l_5(t)$, $t \in [29, 30]$ s, for $\Delta\omega = 5$ rad/s (dashed line), $\Delta\omega = 25$ rad/s (solid line); $\omega_l = 80$ rad/s, $\omega_r = 40$ rad/s, $\psi = \pi/2$; $\omega_j \in \{20.5, 40, 80\}$ rad/s.

After $\tilde{l}_i(t_k)$ are found, the platform points of interest #1–#4 (see Figure 3) displacements $\Delta x_j, \Delta y_j, j = 1, \dots, 4$ on the vertical plane OXY are calculated as follows:

$$\begin{aligned} \Delta x_1(t_k) &= (\tilde{l}_4(t_k) + \tilde{l}_5(t_k))/2, & \Delta y_1(t_k) &= (\tilde{l}_1(t_k) + \tilde{l}_2(t_k) + \tilde{l}_3(t_k))/3, \\ \Delta x_2(t_k) &= (\tilde{l}_4(t_k) + \tilde{l}_5(t_k))/2, & \Delta y_2(t_k) &= (\tilde{l}_2(t_k) + \tilde{l}_3(t_k))/2, \\ \Delta x_3(t_k) &= \tilde{l}_5(t_k), & \Delta y_3(t_k) &= \tilde{l}_3(t_k), \\ \Delta x_4(t_k) &= \tilde{l}_5(t_k), & \Delta y_4(t_k) &= \tilde{l}_4(t_k). \end{aligned}$$

The experimental results for various revolving speeds of rotors and phase shifts are presented below. For the legibility of the graphs, the trajectories are displayed only in the final section of the experiment $t \in [t_a, t_b]$ with a duration of $t_b - t_a$, which is about two characteristic periods of oscillation.

4.2. Case of Identical Rotation Velocities

At first, consider the case when both rotors revolve with the same desired frequency. Namely, let $\omega_l^* = \omega_r^* = 80$ rad/s be taken (i.e., in (3)–(10) parameter $\kappa = 1$ be set). The desired phase shift between the rotors ψ^* is set to zero. The spectral densities for centered

displacements \tilde{l}_2, \tilde{l}_3 of sensors #2, #3, are pictured in Figure 5. As is seen from the plot, the “outstanding” peak on frequency close to 20.5 rad/s appears. It corresponds to the low-frequency resonant mode of the platform. The calculated value of the resonance frequency is quite close to the experimental one, which is confirmed by the Formula (1) for given in [19] values $c_{02} = 5300 \text{ N/m}$, $m_p = 9 \text{ kg}$, $m = 1.5 \text{ kg}$, $\omega_{\text{res},1} = \sqrt{c_{02}/(m_p + 2m)} = 21 \text{ rad/s}$. The appearance of a small oscillation peak in the region of the frequency 1 rad/s can be treated as a manifestation of oscillations arising in the process of the phase shift control.

The motion of the various points of the platform on the vertical plane OXY (where OX stands for the horizon axis, OY denotes the vertical one), are plotted in Figure 6. The time interval for plotting the curves is taken as $t \in 27 + [0.1726, 0.6438] \text{ s}$. This interval corresponds to six periods of motion with a frequency of 80 rad/s.

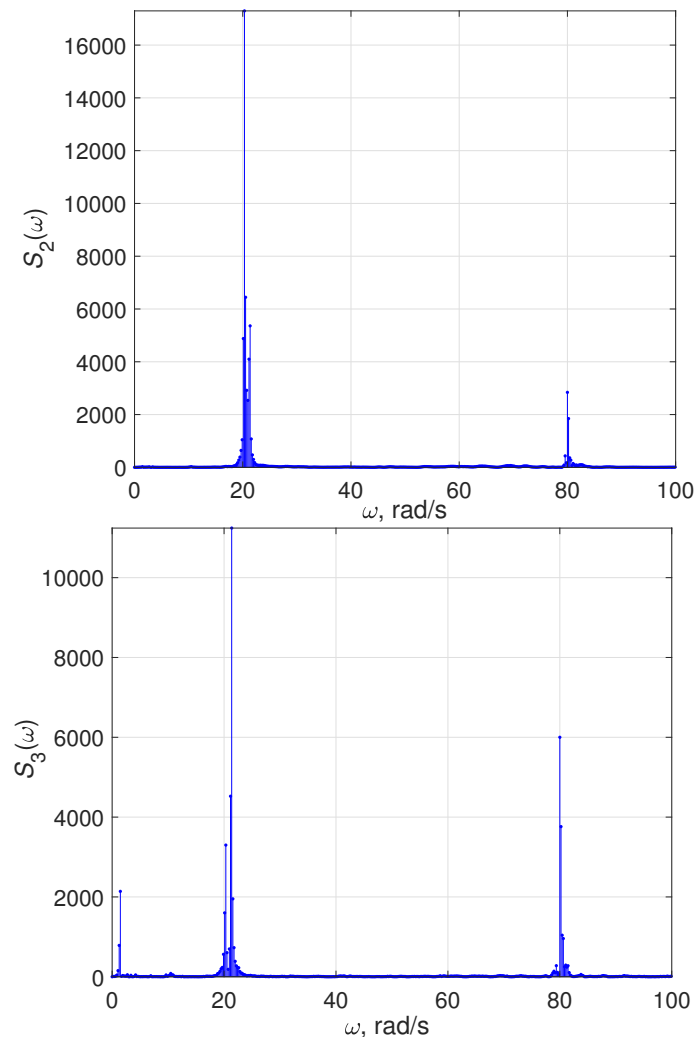


Figure 5. Spectral densities for sensors # 2 and 3, with displacements (in mm). $\omega_l = \omega_r = 80 \text{ rad/s}$, $\psi = 0$.

The upper plots series correspond zero phase shift ($\psi^* = 0$) between the rotors. Respectively, the lower plot is related to phase shift $\psi^* = \pi$. It is seen that the vibration field, having, in general, a similar shape to that in the case of $\psi^* = 0$, changes its inclination. This property can be used for control of the vibrational transportation speed and direction. Of course, for practical application, it is essential what kind of movement the processed stuff acquires. This dependence can be quite complex and determined not only by the platform movement but also by the physical characteristics of the substance. Some preliminary analysis is contained in the works [15–17], but it is not exhaustive and does not cover the whole variety of vibration fields that can be provided by the method proposed here. The

studies conducted show its potential and a necessity to be continued for real machines and situations.

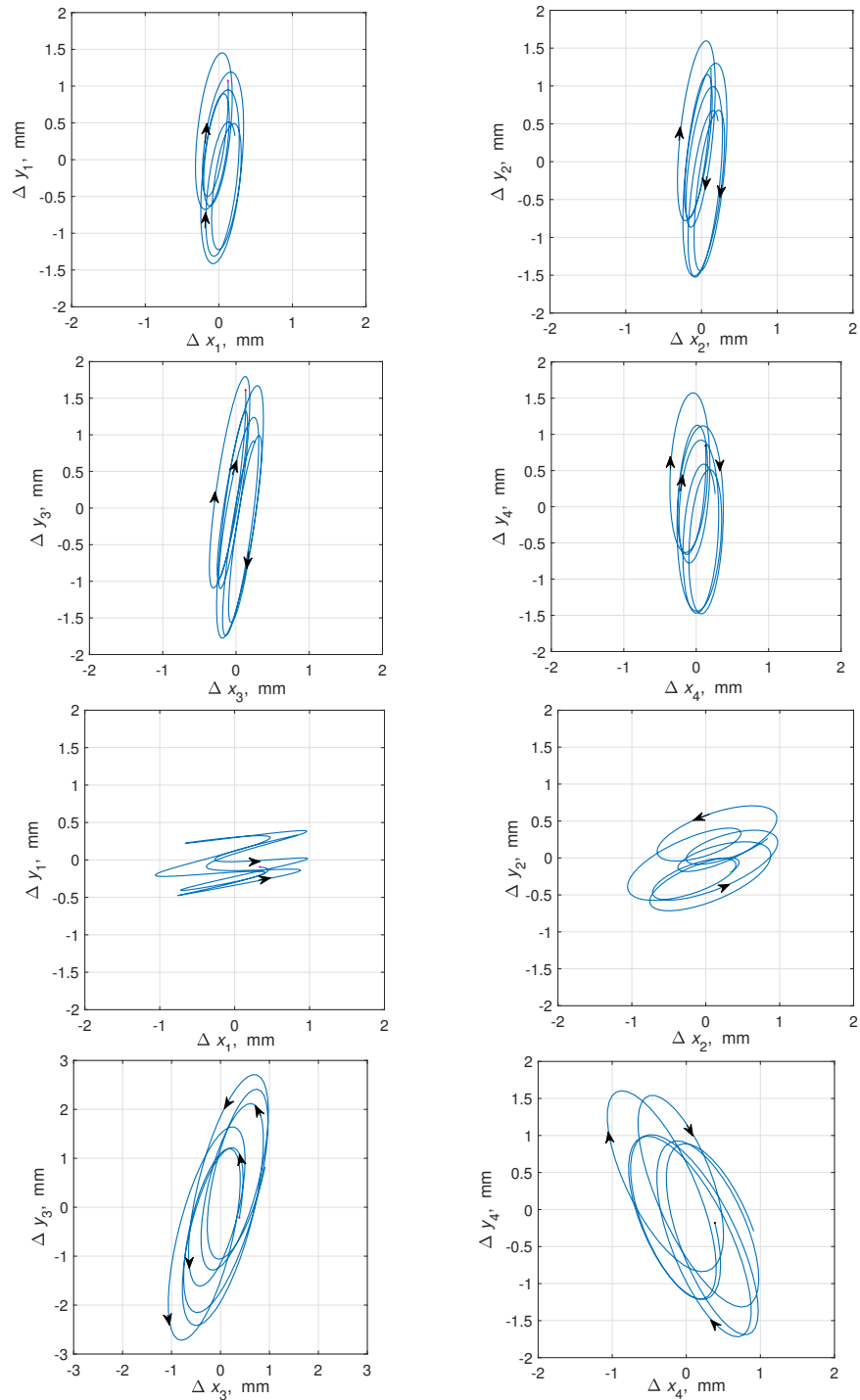


Figure 6. Vibration fields in the platform sections #1–#4. $\omega_l = \omega_r = 80$ rad/s. Upper plot: $\psi = 0$. Lower plot: $\psi = \pi$ rad.

4.3. Case of Different Rotation Velocities

Additionally, similar experiments were performed for the case of different rotation frequencies of rotors. Namely, $\omega_l^* = 90$ rad/s and $\omega_r^* = 45$ rad/s were taken (i.e., in (3)–(10) parameter $\kappa = 2$ was set). The desired phase shift between the rotors ψ^* is set to zero. The corresponding spectral densities for centered displacements \tilde{l}_2, \tilde{l}_3 of sensors #2, #3 are pictured in Figure 7. As is seen from the plot, the spectrograms have three peaks: on the

frequencies of 45 rad/s, 90 rad/s, corresponding the rotation velocities of the drives, and the peak on 20 rad/s appears related to the natural oscillating of the platform.

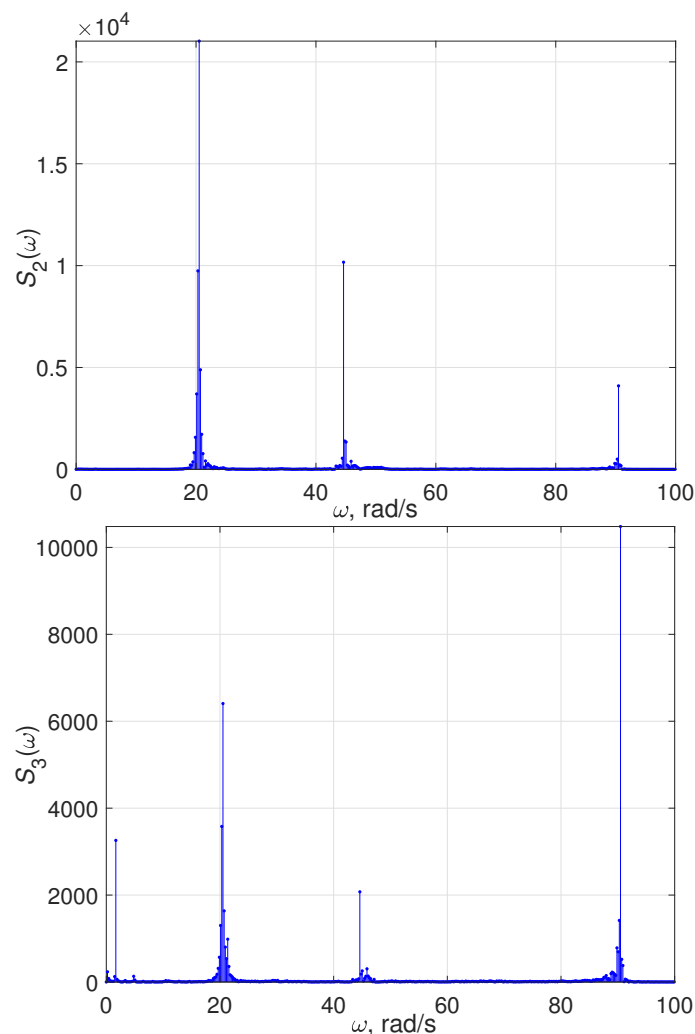


Figure 7. Spectral densities for sensors # 2 and 3, with displacements (in mm). $\omega_l = 90$ rad/s, $\omega_r = 45$ rad/s, $\psi = 0$.

The corresponding vibration fields of the platform sections #1–#4 on the vertical plane OXY are plotted in Figure 8. The time interval for plotting the curves is taken as $t \in 27 + [0.4867, 0.9056]$ s. This interval corresponds to six periods of motion with a frequency 90 rad/s. The platform motion is for the considered multiple synchronization case, which is more complex compared with the single-frequency one due to interference both from the slow oscillations with the natural frequency of the platform (20 rad/s) and two rotation speeds of the drives with different values (90 and 45 rad/s).

The upper plots in Figure 8 correspond to zero phase shift ($\psi^* = 0$) between the rotors, while the lower plot is related to phase shift $\psi^* = \pi$. It is seen that the vibration field is more complex than in the single-frequency case and also varies with the phase shift, set between the rotors. This gives additional flexibility in control of the platform vibration fields and can be used in developing smart vibrational technologies.

As for the coincident frequencies considered in the previous subsection, and for different frequencies, the results for which are presented here, it is clear that by changing the phase shift it is possible to significantly tune the vibration fields. The desired type of field depends on specific conditions and needs to be studied from a technological point of view. However, according to the obtained graphs, it is clear that the conclusion made based on simulations in [19], that in the case of the double synchronous mode the ordinate

of the lower point of the trajectory is lower than in the case of the single synchronous mode, is confirmed experimentally, which improves the efficiency of unloading and prevents congestion formation (see plots $(\Delta x_4, \Delta y_4)$ in Figure 8, right column).

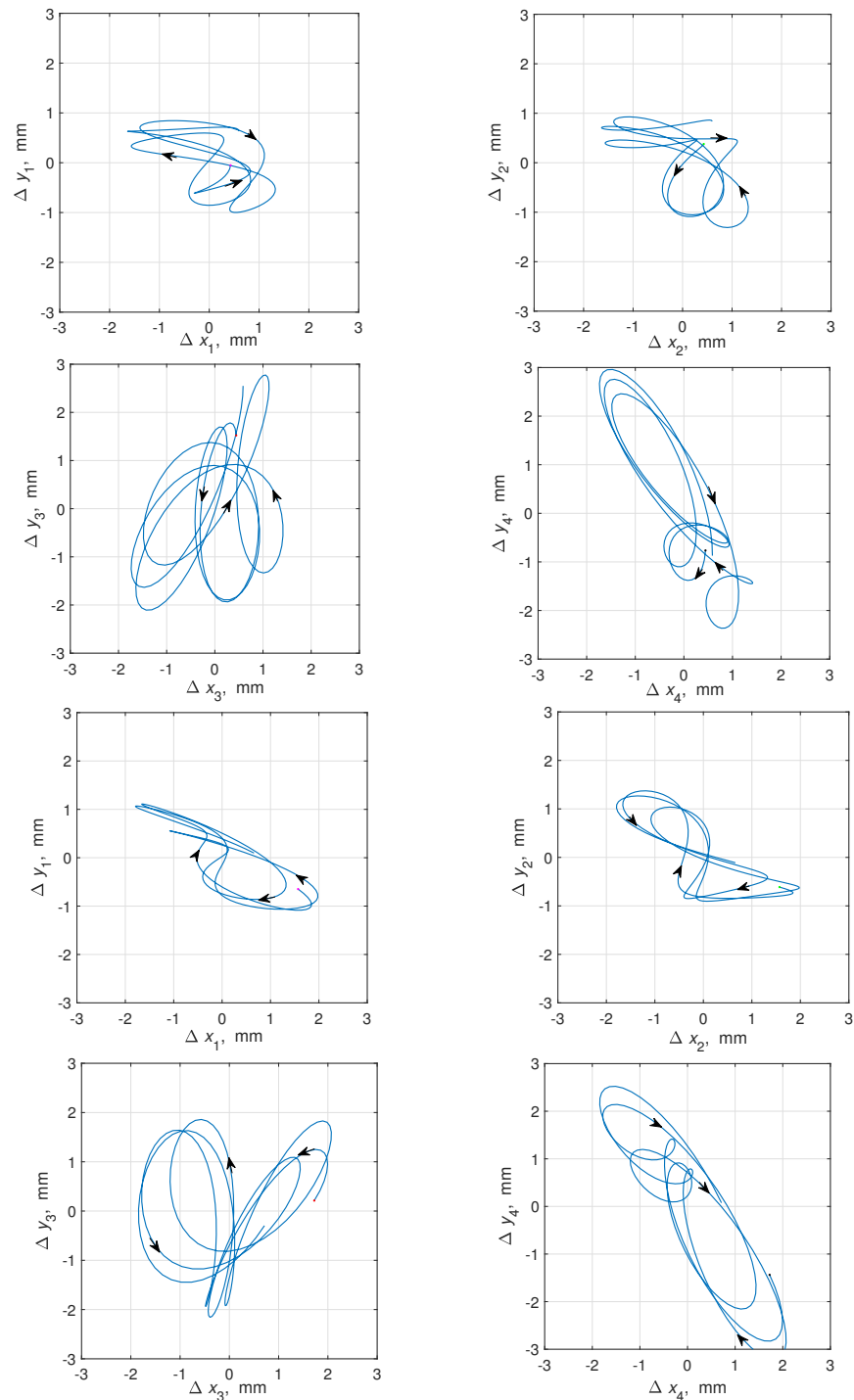


Figure 8. Vibration fields in the platform sections #1–#4. $\omega_l = 90$ rad/s, $\omega_r = 45$ rad/s. Upper plot: $\psi = 0$. Lower plot: $\psi = \pi$ rad.

5. Conclusions

The paper demonstrates the possibility of using controlled multiple synchronization of unbalanced rotors driven by induction motors to form vibration fields in the working platform of a vibration mechatronic setup. The experimental results obtained at the MMLS SV-2M of the IPME RAS are presented, demonstrating the efficacy of the proposed approach. The

method proposed here obviously leads to simpler algorithms than in [19] which simplifies its implementation but makes the system rougher, without the possibility of fine-tuning.

Expanding the capabilities of controlled synchronization can be achieved by employing unidirectional (master–slave synchronization). Since the control method using a PI controller may be insufficient, especially in theoretical research, the alternative control methods including adaptive control, variable-structure control on sliding-mode, speed gradient techniques, Neural Networks, nonlinear correction methods, Field-Oriented Control (FOC) or Linear Quadratic Regulator (LQR), could be employed in future investigations, representing promising areas for further research.

Author Contributions: Conceptualization, O.P.T.; data curation, I.Z.; formal analysis, A.L.F. and B.A.; funding acquisition, A.L.F.; investigation, I.Z.; methodology, B.A.; project administration, A.L.F.; software, I.Z.; supervision, B.A.; writing—original draft, A.L.F. and B.A.; writing—review and editing, B.A. and O.P.T. All authors have read and agreed to the published version of the manuscript.

Funding: The research was supported by the Ministry of Science and Higher Education of the Russian Federation (project no. 124041500008-1).

Institutional Review Board Statement: Not applicable.

Data Availability Statement: No new data were created or analyzed in this study. Data sharing is not applicable to this article.

Acknowledgments: The authors are grateful to V. I. Boikov for his invaluable work in creating the electronic and computer facilities of the MMLS SV-2M.

Conflicts of Interest: The authors declare no conflicts of interest.

Abbreviations

The following abbreviations and notations are used in this manuscript:

AC	Alternating Current
DFT	Discrete Fourier Transform
DoF	Degrees of Freedom
IDFT	Inverse Discrete Fourier Transform
IM	Induction Motor
FOC	Field-Oriented Control
HDD	Hard Disk Drive
LQR	Linear Quadratic Regulator
MFC	Macro Fiber Composite
MMLS	Multiresonance Mechatronic Laboratory Setup
PI	Proportional–integral
VM	Vibration Machine

References

1. Blekhman, I.I. *Vibrational Mechanics: Nonlinear Dynamic Effects, General Approach, Applications*; World Scientific: Singapore, 2000.
2. Braun, S.; Ewins, D.; Rao, S. *Encyclopedia of Vibration*; Academic Press: San Diego, CA, USA, 2002.
3. Blekhman, I.I.; Vaisberg, L.A. Self-Synchronization as a Self-Organization Phenomenon and a Basis for Development of Energy-Efficient Technologies. In Proceedings of the 10th Biennial International Conference on Vibration Problems (ICOVP), Prague, Czech Republic, 5–8 September 2011; Segla, S., Tuma, J., Petrikova, I., Eds.; Springer: Berlin/Heidelberg, Germany, 2011; pp. 365–370.
4. Li, L.; Chen, X. Multi-frequency Vibration Synchronization and Stability of the Nonlinear Screening System. *IEEE Access* **2019**, *7*, 171032–171045. [[CrossRef](#)]
5. Blekhman, I.I.; Landa, P.S.; Rosenblum, M.G. Synchronization and chaotization in interacting dynamical systems. *Appl. Mech. Rev.* **1995**, *48*, 733–752. [[CrossRef](#)]
6. Blekhman, I.I.; Yaroshevich, N.P. Extension of the domain of applicability of the integral stability criterion (extremum property) in synchronization problems. *J. Appl. Math. Mech.* **2004**, *68*, 839–846. [[CrossRef](#)]
7. Xu, Z.Q.; Meng, Z.R.; Xue, S.H.; Zhang, D.Q.; Du, F.S. Effect of Oscillation Parameters to Flow Field in the Pool during the Oscillating Twin-Roll Strip Casting Process. *Chin. J. Mech. Eng.* **2018**, *31*, 99. [[CrossRef](#)]
8. Liu, Y.; Wang, T.; Gong, G.; Gao, R. Present Status and Prospect of High-Frequency Electro-hydraulic Vibration Control Technology. *Chin. J. Mech. Eng.* **2019**, *32*, 93. [[CrossRef](#)]

9. Shi, S.; Hou, Y.; Fang, P.; Hou, D.; Peng, H. Synchronization investigation on space vibration system driven by two vibrators with arbitrary direction axes. *Appl. Math. Model.* **2023**, *120*, 199–216. [[CrossRef](#)]
10. Altshul, G.; Gousskov, A.; Panovko, G.; Shokhin, A. Dynamics features of a vibrating machine with elastic element having exponential characteristic of resilient force. *Cybern. Phys.* **2021**, *10*, 59–62. [[CrossRef](#)]
11. Panovko, G.; Shokhin, A.; Ereimeikin, S. The control of the resonant mode of a vibrating machine that is driven by an asynchronous electro motor. *J. Mach. Manuf. Reliab.* **2015**, *44*, 109–113. [[CrossRef](#)]
12. Liu, Y.; Zhang, X.; Gu, D.; Jia, L.; Wen, B. Synchronization of a Dual-Mass Vibrating System with Two Exciters. *Shock Vib.* **2020**, *2020*, 9345652. [[CrossRef](#)]
13. Zhang, X.; Zhang, X.; Zhang, C.; Wang, Z.; Wen, B.C. Multiple-frequency synchronization of the four exciters in a far super-resonant vibrating system with an isolation frame. *J. Low Freq. Noise Vib. Act. Control* **2021**, *41*, 646–658. [[CrossRef](#)]
14. Leniowska, L.; Sierże, M. Vibration control of a circular plate using parametric controller with phase shift adjustment. *Mechatronics* **2019**, *58*, 39–46. [[CrossRef](#)]
15. Blekhman, I.I.; Dzhanelidze, G.Y. *Vibrational Movement [Vibratsionnoye Peremeshcheniye]*; Nauka: Moscow, Russia, 1964. Available online: <https://www.naukapublishers.ru> (accessed on 8 August 2024). (In Russian)
16. Lyan, I.; Panovko, G. Modelling the granular medium dynamics on rough vibrating plane using method of large particles. *IOP Conf. Ser. Mater. Sci. Eng.* **2019**, *489*, 012039. [[CrossRef](#)]
17. Blekhman, I.I.; Vasil'kov, V.B.; Semenov, Y.A. Vibrotransporting of Bodies on a Surface with Non-Translational Rotational Oscillations. *J. Mach. Manuf. Reliab.* **2020**, *49*, 280–286. [[CrossRef](#)]
18. Fradkov, A.L.; Tomchina, O.P.; Andrievsky, B.; Boikov, V.I. Control of Phase Shift in Two-Rotor Vibration Units. *IEEE Trans. Control Syst. Technol.* **2021**, *29*, 1316–1323. [[CrossRef](#)]
19. Tomchina, O.P. Vibration field control of a two-rotor vibratory unit in the double synchronization mode. *Cybern. Phys.* **2022**, *11*, 246–252. [[CrossRef](#)]
20. Vinogradov, O. *Fundamentals of Kinematics and Dynamic of Machines and Mechanisms*; CRC Press LLC.: Boca Raton, FL, USA; London, UK; New York, NY, USA; Washington, DC, USA, 2000.

Disclaimer/Publisher's Note: The statements, opinions and data contained in all publications are solely those of the individual author(s) and contributor(s) and not of MDPI and/or the editor(s). MDPI and/or the editor(s) disclaim responsibility for any injury to people or property resulting from any ideas, methods, instructions or products referred to in the content.